Letters in Applied NanoBioScience
Open-Access Journal (ISSN: 2284-6808)

Article
Volume 15, Issue 2, 2026, 59
https://doi.org/10.33263/LIANBS152.059

Structural and Functional Properties of Cellulose/Mg–Al Layered Double Hydroxide Biocomposites: Effects of Synthesis Methods and Thermal Stability

Soumia Mekdad [1], Hamid Ziyat [1], Jamal Houssaini [1,*], Mohammed Naciri Bennani [1], Marwa Alaqarbeh [2]

1 Laboratory of Chemistry-Biology Applied to the Environment, URL–CNRST N°13, Research Team "Materials and Applied Catalysis", Chemistry Department, Faculty of Sciences, Moulay Ismail University, BP. 11201 Zitoune, Meknes 50000, Morocco; soumiamek31@gmail.com, (S.M.); ziyat.hamid@gmail.com, (H.Z.); jamal.houssaini@edu.umi.ac.ma (J.H.), m.naciribennani@umi.ac.ma (M.N.B.).
2 Basic Science Department, Prince Al Hussein bin Abdullah II Academy for Civil Protection, Al-Balqa Applied University, Al-Salt 19117, Jordan; marwa.alaqarbeh@narc.gov.jo (M. A).
* Correspondence**:** jamal.houssaini@edu.umi.ac.ma;

Received: 12.05.2026; Accepted: 21.02.2026; Published: 30.06.2026

Abstract: Microcrystalline cellulose (CL) extracted from biomass was combined with Mg–Al layered double hydroxides (LDH) to develop sustainable hybrid biocomposites using different synthesis routes. The influence of the preparation method and calcination temperature on the structural evolution and thermal properties of the resulting CL/LDH materials was systematically investigated by X-ray diffraction (XRD), Fourier-transform infrared spectroscopy (FTIR), and differential thermal analysis (DTA). The comparative evaluation of the synthesis strategies revealed their significant impact on phase transformations and structure–property relationships. Among the prepared materials, the CL/LDH-SDS biocomposite exhibited the highest thermal stability, owing to the synergistic effect of sodium dodecyl sulfate (SDS) intercalation and the layered LDH architecture. These findings demonstrate that optimizing the synthesis route and thermal treatment is an effective strategy for tailoring the structural integrity and thermal performance of cellulose/LDH biocomposites, highlighting their potential as sustainable functional materials.

Keywords: Layered double hydroxide; Cellulose; Biocomposites; Structural; Thermal stability.

1. Introduction

Biocomposites represent a vital and rapidly evolving class of advanced materials that have attracted significant attention in recent years for their remarkable performance and multifunctionality [1]. These hybrid materials, which combine a polymer matrix with nanoscale fillers such as layered silicates, carbon nanotubes, graphene, or metal oxides, offer an outstanding balance of mechanical strength, thermal stability, barrier properties, and flame-retardant performance even with minimal filler content. Among them, clay-based nanocomposites have emerged as particularly promising due to their cost-effectiveness, abundance, and ease of incorporation into polymer matrices.

Incorporating a small fraction of clay into polymers such as poly(methyl methacrylate) (PMMA), poly(ethylene terephthalate) (PET), polypropylene (PP), epoxy

resins, polyimides, or ethylene vinyl acetate (EVA) can dramatically improve the composites' properties. Therefore, researchers and industry players should explore the potential of nanocomposites in various applications to enhance the performance of various systems and products [2–4]. Using biodegradable polymers as a matrix for nanocomposites is a relatively new development. Some of the main biodegradable polymers used for this purpose include poly (3-caprolactone), poly (lactic acid), cellulose and its derivatives, starch, and poly (hydroxybutyrate). Cellulose, the most abundant and naturally occurring polymer, is often preferred due to its biodegradability and affordability [5,6].

Recent studies have increasingly focused on cellulose as a sustainable polymer matrix for the development of advanced composites, with particular emphasis on improving its structural and functional properties. In 2012, Yang *et al*. synthesized cellulose/montmorillonite nanocomposites by incorporating clay nanofillers into the cellulose matrix, yielding transparent, flexible films with enhanced mechanical strength and excellent gas barrier properties. These characteristics make such materials promising candidates for various high-performance applications [7]. In another example, Khan *et al*. created antibacterial nanocomposites by dispersing ZnO nanoparticles in the cellulose acetate matrix in 2014 [8]. A study conducted by Delhom *et al*. in 2010 demonstrated the use of cellulose-based cotton and layered silicate clay nanocomposites to enhance the flame-retardant properties of cellulose. The addition of nanocomposites resulted in a significant improvement in thermal properties compared to cellulose alone, due to degradation temperature by 45°C [9]. Other researchers have also improved cellulose's thermal properties by adding clay nanofillers within a polymer matrix. Liu *et al*. developed three-component nanocomposite films by combining sodium montmorillonite clay (MTM), a relatively high molecular weight water-soluble cellulose derivative (carboxymethyl-cellulose CMC), and nano-fibrillated cellulose (NFC) from pulp wood, which displayed favorable flame-retardant characteristics [10].

Our group conducted several studies to improve the properties of cellulose/clay nanocomposites based on a microcrystalline cellulose matrix and MgAl–LDH as clay nano-charges. The current study aims to observe the structural changes of these nanocomposites at different temperatures and determine the effect of Hydrotalcite nanofillers on their thermal resistance. The researchers developed CL/LDH nanomaterials using composite-P1 via direct coprecipitation, composite-P2 after swelling CL and LDH in an aqueous solution, and composite-P3 via sonification [11]. A new method has been developed that involves modifying Hydrotalcite with a surfactant, specifically sodium dodecyl sulfate (SDS), before combining it with CL and swelling the mixture with distilled water. The obtained material was denoted composite-P4-SDS. The resulting nanocomposites were subjected to thermal treatments at temperatures ranging from ambient to 600 °C in increments of 100 °C. The samples obtained at each temperature were immediately analyzed by XRD, FTIR spectroscopy, and DTA to monitor their structural evolution and thermal stability.

2. Materials and Methods

2.1. Materials.

Microcrystalline cellulose was purchased from Sigma-Aldrich. Metal salts, including magnesium chloride hexahydrate ($MgCl_2 \cdot 6H_2O$), magnesium nitrate hexahydrate ($Mg(NO_3)_2 \cdot 6H_2O$), aluminum chloride hexahydrate ($AlCl_3 \cdot 6H_2O$), and aluminum nitrate

nonahydrate ($Al(NO_3)_3 \cdot 9H_2O$), were obtained from LOBA Chemie with a purity of 99%. Sodium hydroxide (NaOH) in pearl form (98% purity), sodium carbonate (Na_2CO_3, 99.9% purity), and sodium dodecyl sulfate (SDS, 99.8% purity) were also provided by LOBA Chemie. Urea (99% purity) was supplied by Chemical.

2.2. Methods.

The material's powder XRD was obtained using a Philips PW (1800) X-ray diffractometer set to 40 kV and 20 mA, and equipped with Cu K_α = 1,5418 Å radiation. At a scan rate of one degree per minute, the spectra of the various samples were recorded in a 2θ range covering 5° to 70° with an angular increment of 0.04°. To obtain the FTIR spectrum of the material, a Michelson interferometer was used to separate the ceramic source and detector TGS in a JASCO 4100 FTIR spectrophotometer. Using the KBr pellet method, the sample's FTIR spectrum was acquired. The pellet was made at a pressure of 5 tons, and the sample to KBr ratio was 1:50. With a resolution of 20 cm^{-1}, the matching spectra were obtained between 400 and 4000 cm^{-1}. The Shimadzu TA-60 type apparatus was used for Thermal analysis (DTA) in air with a linear heating rate of 10°C.min^{-1} from ambient temperature to 600°C. The calcinations were done in a furnace in a flow of air. The temperature was raised at a rate of 5°C/min to reach 600°C and maintained for 8h.

2.2.1. Preparation of $MgAlCO_3$–LDH.

The solid $MgAlCO_3$ Hydrotalcite was prepared using a simple coprecipitation method at pH = 10 [12]. A 60.99g of ($MgCl_2 . 6H_2O$) and 24.14g of ($AlCl_3 . 6H_2O$) in 300 ml of distilled water were dissolved to make a caustic solution by dissolving 300 ml of water, 32g of NaOH, and 2.12g of Na_2CO_3. These two solutions were slowly added while vigorously stirring to keep the pH constant at 10. The mixture was refluxed at 70°C for 17h under the same vigorous stirring. The resulting solid was collected, washed with hot distilled water, and dried at 70°C for 15h.

2.2.2. Intercalation of $MgAlNO_3$–LDH by SDS.

The coprecipitation method at constant pH was used to modify the Hydrotalcite by mixing two solutions: the first solution contains salts of aluminum nitrate (7.5g of $Al(NO_3)_3 . 9H_20$) and magnesium nitrate (15.4g $Mg(NO_3)_2 . 6H_2O$) along with 7g of sodium dodecyl sulfate (SDS) in 100 ml of distilled water. The second solution is NaOH (6g dissolved in 100 ml of distilled water). While maintaining the pH at a constant value of 10, both solutions were added dropwise under a nitrogen atmosphere while stirring. After the addition, the reaction mixture was stirred for 12h at 75°C. The solid obtained after centrifugation, washing with distilled water, and drying at 70°C was noted as LDH-SDS.

2.2.3. Preparation of the biocomposites CL/LDH.

The CL-LDH nanomaterials were synthesized using four state-of-the-art protocols, including $MgAlCO_3$–LDH or $MgAlNO_3$-LDH, denoted MgAl–LDH, as nanomaterials. Herein are the possibilities of CL-LDH synthesis and the benefits of this cutting-edge innovation.

a-Protocol 1: The initial step involved dispersing $MgAlCO_3$–LDH clay fillers in a solution containing NaOH, urea, and microcrystalline cellulose. The CL solution was

prepared using the methodology outlined by Jia *et al*. [13]. Specifically, a mixture of 28g of NaOH and 48g of urea was vigorously stirred in 320 ml of distilled water, followed by the addition of 8.14g of CL. The resultant mixture was stirred for 12h and then cooled to 5°C in a refrigerator. This cellulose solution was employed in the synthesis of CL–LDH biocomposites. In the nanocomposite synthesis, 5% of $MgAlCO_3$–LDH was dispersed in a 95% cellulose solution (w/w).

The reaction mixture was left under agitation overnight. Subsequently, the solution underwent microwave radiation at 350W for 3min, following previously determined optimal conditions [14,15]. The mixture was then centrifuged at 3000 rpm for 12min, and the synthesized product was washed with a mixture of distilled water and ethanol (50V/50V) before being dried in an oven at 50°C for 7h and the final product was denoted Composite-P1.

b-Protocol 2: In this protocol, 0.1g of $MgAlCO_3$–LDH and 1.9g of cellulose were separately soaked in distilled water. The solutions were stirred for 2h and mixed at 40°C for 18h. Microwave energy was then applied to the solution for 3 minutes at 350W. The resultant composite CL-$MgAlCO_3$–LDH had a creamy texture. The product was separated from the solution by centrifugation for 12min at 3500 rpm and then washed with distilled water and ethanol. Finally, it dried at 60°C, where the sample was denoted Composite-P2.

c-Protocol 3: NaOH, urea, and H_2O solution was prepared by adding 3.5g of NaOH, 6g of urea, and 40mg of H_2O to a known amount of $MgAlCO_3$–LDH. The solution underwent stirring for a duration of 2h at room temperature, followed by the sonication of the $MgAlCO_3$–LDH suspension for a period of 8 min. Subsequently, the solution was cooled to 7°C. The ultrasonic treatment parameters were set to Energy: 29254J, Power: 65W, Time: 8, 36, 50 continuous seconds, with 10 seconds off intervals. A predetermined amount of CL was added to the solution to yield a composite comprising 95% CL and 5% LDH. The resulting mixture was stirred overnight, subjected to centrifugation at 3500 rpm for 12min, and rinsed with a water/ethanol solution. Finally, the sample was dried at 60°C and named Composite-P3.

d-Protocol 4: The CL-LDH–SDS nanocomposite was synthesized by separately swelling 0.1 g of $MgAlNO_3$-LDH–SDS and 1.9g of CL in distilled water and stirring the solutions for 2h. Subsequently, the swollen samples were combined and stirred at 40°C for 18 hours. Microwave energy was then applied to the solution for 3 min at 350 W, creating a creamy-textured CL-LDH-$MgAlNO_3$–SDS nanocomposite. The product was separated from the solution by centrifugation for 12 min at 3500 rpm and was subsequently washed with distilled water and ethanol. Finally, the product was dried at 60°C and CL-LDH–SDS (Composite-P4-SDS).

3. Results and Discussion

3.1. XRD analysis.

The X-ray diffraction (XRD) pattern of MgAl–LDH ($MgAlCO_3$/$MgAlNO_3$) is presented in Figure 1a. The diffraction peaks (00l) observed in the pattern are characteristic of a lamellar structure like those reported in previous studies. These peaks indicate that the synthesized MgAl-LDH is a pure and well-crystallized LDH phase as Hydrotalcite type [16,17]. In the case of calcined LDH, the (003) peak remains delicate and intense up to 300°C, indicating that the lamellar character of the structure was maintained up to this

temperature. Between 300°C and 400°C, the disappearance of the (003) and (110) peaks indicates the beginning of the destruction of the lamellar structure. Above 400°C, two new peaks emerge at 2θ = 43° and 63°, indicating the appearance of the mixed oxide $Mg_3AlO_4(OH)$ [18]. The XRD pattern of CL is presented in Figure 1b. Three diffraction peaks are observed at 2θ = 16°, 22°, and 34°, which are assigned to (110), (002), and (004) diffraction planes, respectively [19]. The peak at 2θ = 16° corresponds to hemicellulose (amorphous phase), while the peaks at 2θ = 22° and 34° correspond to the crystalline phase of cellulose [20]. No change is observed in the pattern up to 300°C. The peak of the amorphous phase disappears at 400°C, and that of the crystalline phase becomes less intense and broader at this temperature due to the beginning of decomposition of the crystalline phase. It coincides with the thermal analysis DTA, which revealed two CL decomposition peaks around 370°C and 475°C.

The XRD pattern of the Composite-P1 (Figure 1c) was characterized by the presence of the two phases (LDH and CL). On the spectra at ambient temperature of this compound, we observed another peak at 2θ = 20°, which maintained up to 300°C and which shows the presence of the cellulose phase in a weak polymerization degree (PD: Degrees of cellulose polymerization), in agreement with the result obtained by J. Holladay and Z. C. Zhang [21]. In our case, this suggests that the dissolution of the CL in the NaOH/urea medium is unfavorable for the dispersion of cellulose in the MgAl–LDH phase, and the CL would be in a weakly polymerized state. Up to 300°C, the composite keeps the same behavior as MgAl–LDH alone since the peak (003) remains intense and the lamellar character is preserved. However, at 400°C, an intermediate phase was formed before forming the mixed oxide at 500°C. Changes in coloring accompanied these variations. At 400°C, the nanocomposite has taken a black color, which indicates that the organic matter is burnt, and at 500°C, a grey color was observed. In comparison, at 600°C, the composite resumed the whitish color: organic matter has disappeared.

Figure 1d represents the XRD pattern of the CL–LDH nanocomposite synthesized according to the P2 process (composite-P2). This material has a partially exfoliated structure characterized by the dominant presence of the peaks of the CL. The presence of the principal peak (003) of MgAl–LDH with a very low intensity suggests the existence of MgAl–LDH crystallites. No change was observed up to 300°C. The CL in this structure adopts the same behavior as when alone. From 400°C, the CL's disappearance begins, and the mixed oxide $Mg_3AlO_4(OH)$ forms until the CL collapses completely at 600°C.

The XRD pattern of the nanocomposite developed by the ultrasound method (composite-P3) is presented in Figure 1e. This composite was characterized by the presence of two phases (CL and MgAl–LDH), and the peaks are intense, well-resolved, and symmetrical. The peak at 2θ = 22° includes the crystalline CL and the (006) peak of the MgAl–LDH. This nanocomposite remains stable up to 400 °C. From 500°C, the mixed oxide appears with additional peaks corresponding to the spinel phase ($MgAl_2O_4$). The latter is generally observed for calcination temperatures above 600 °C [22]. It suggests that the LDH phase in this nanocomposite is less stable, while the CL keeps its structure up to 400°C. The presence of the peak around 2θ = 11° (peak 003) on the spectra of the samples calcined at 500°C and 600°C compared to composite-P1 and composite-P2, may be due to the presence of the crystals of the MgAl-LDH hidden by the CL, which reappear after decomposition of the cellulose at 400°C.

Figure 1f shows the XRD pattern of the nanocomposite CL-LDH–SDS (Composite-P4-SDS). We note the presence of the characteristic peaks of the CL and a remarkable absence of those of the MgAl–LDH, which indicates that this nanocomposite has an exfoliated structure [11]. Cellulose is present up to 400°C, which indicates a gain in thermal stability of 100°C for the nanomaterial modified by SDS compared to the polymer alone. It shows that the clay nanofillers modified by SDS improve the stability of the polymer.

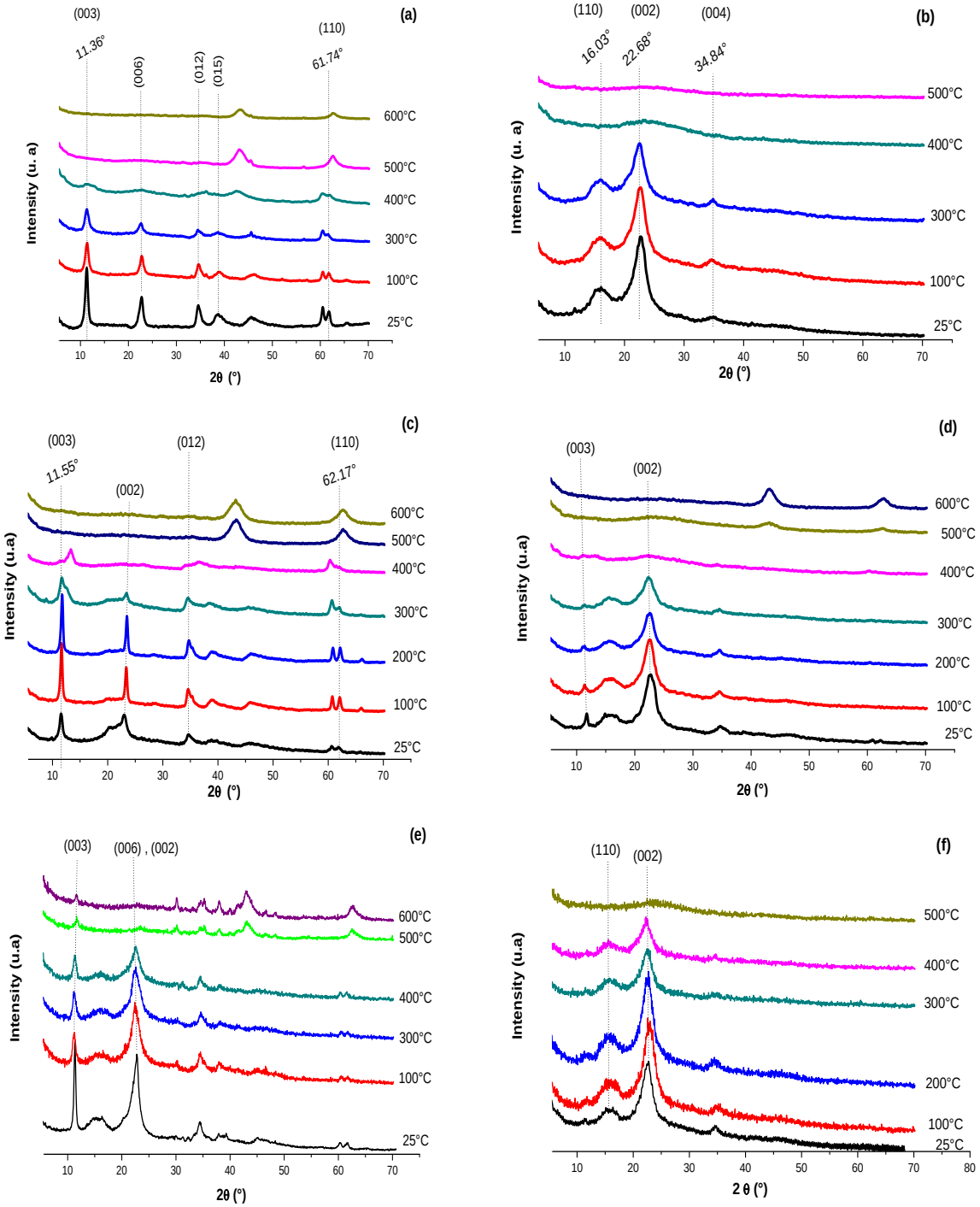

Figure 1. XRD patterns of the non-calcined and calcined samples after thermic treatments at 100°C, 300°C, 400°C, 500°C, and 600°C: **(a)** MgAl-LDH; **(b)** CL; **(c)** composite-P1; **(d)** composite-P2; **(e)** composite-P3; **(f)** composite-P4-SDS.

3.2. FTIR analysis.

The FTIR spectra of MgAl–LDH, microcrystalline cellulose, and the synthesized biocomposites are analyzed in Figure 2, both before and after calcination.

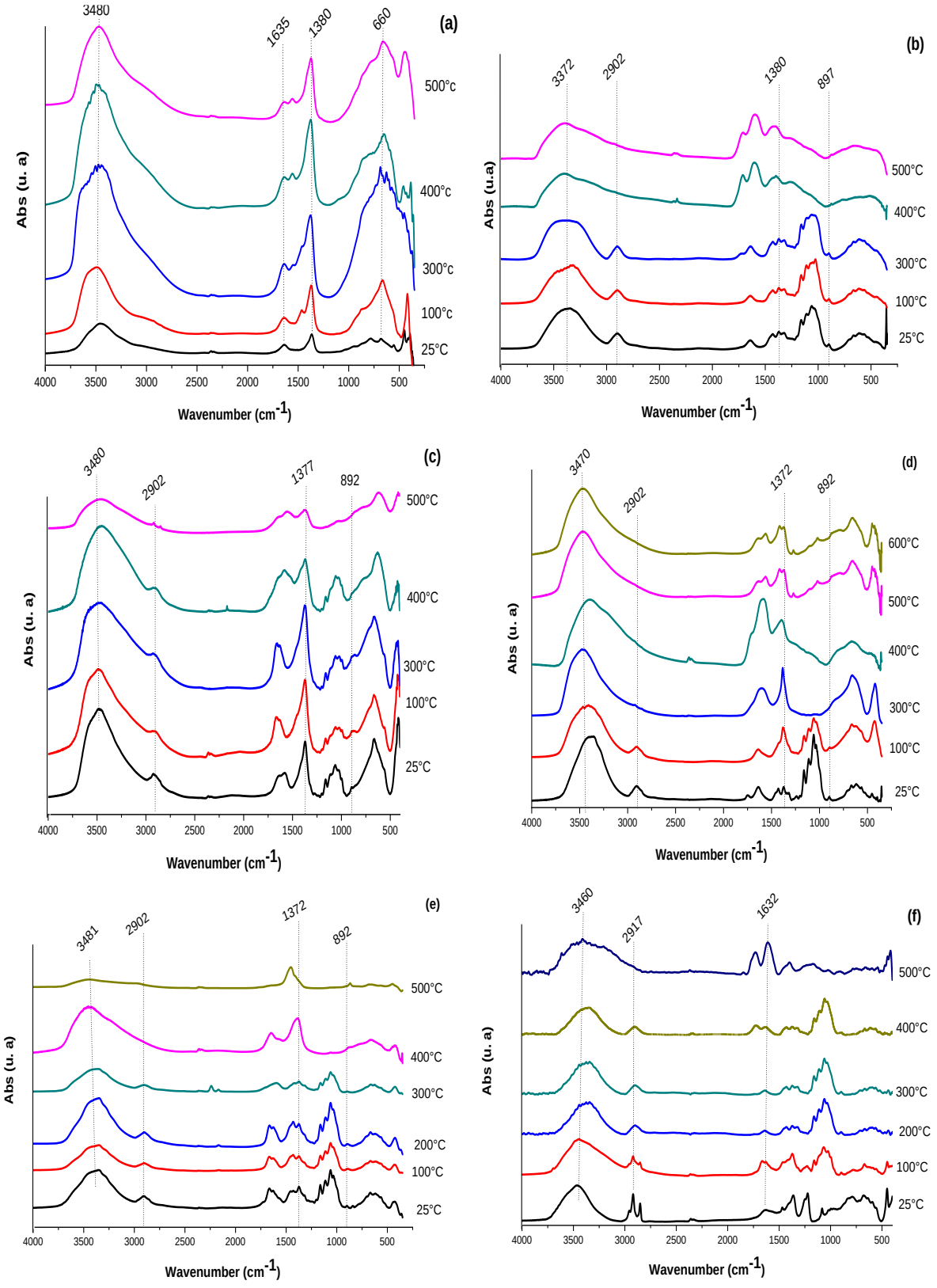

Figure 2. FTIR spectra of the various samples before and after calcination: **(a)** MgAl–LDH; **(b)** CL; **(c)** Composite-P1; **(d)** Composite-P2; **(e)** Composite-P3; **(f)** Composite-P4-SDS.

The MgAl–LDH spectrum, as depicted in Figure 2a, displays the characteristic MgAl–LDH bands in the range of 450-900 cm^{-1} with ν(M-O) and ν(M-O-M) (M = Al, Mg) [23,24]. The prominent bands include ν(OH) at 3480 cm^{-1}, δ(H_2O) at 1635 cm^{-1}, and ν(NO_3^-) for $MgAlNO_3$ and ν(CO_3^{2-}) for $MgAlCO_3$ at 1380 cm^{-1}. In contrast, the CL spectrum in Figure 2b demonstrates a broad band centered at 3372 cm^{-1}, corresponding to the stretching vibrations of –OH groups. The absorption bands between 1000 and 1200 cm^{-1} are attributed to the C-O stretching on the polysaccharide skeleton. The band at 2902 cm^{-1} corresponds to C-H vibrations in cellulose, which causes the deformed band at 1380 cm^{-1}. Analysis of FTIR spectra provides valuable information on the chemical composition and structure of the materials under investigation. The results demonstrate the presence of characteristic MgAl–LDH and CL bands, confirming the successful synthesis of the biocomposites [11].

The band observed on the spectrum of MgAl–LDH around 3400 cm^{-1} (Figure 2) corresponds to vibrations valence of the OH–(OH··OH) groups of physiosorbed water and OH–(M–OH) groups (M = Mg^{2+}, Al^{3+}) and to O–H of water molecules between sheets [25], increases in intensity because it covers both the O–H band of the hydroxyl groups of the layers brucite-type of MgAl–LDH and the vibration of elongation of the O–H bonds of the alcohol functions of the cellulose [26]. The FTIR spectra of calcined composites reveal a decrease in intensity of the bands around 3400 cm^{-1} and 1630 cm^{-1}, corresponding to dihydroxylation and dehydration of MgAl–LDH. The absorption bands located around 2900 cm^{-1} and 890 cm^{-1}, observed on the spectra of the composites, are respectively associated with the C-H stretching vibration of cellulose [27] and the anti-symmetrical stretching vibrations of the C-O-C glycosidic linkage [28]. The evolution of the intensity of these two bands was followed as a function of the calcination temperature. We note that these bands gradually decrease in intensity when the calcination temperature increases and disappear entirely at 400°C for the Composite-P1, Composite-P2, and Composite-P3 (Figure 2c, Figure 2d, and Figure 2e), except for the Composite-P4-SDS. For this nanocomposite, the bands at 2902 and 897 cm^{-1} were preserved up to 500°C (Figure 2f) and revealed that the microcrystalline cellulose, which degrades at 400 °C, is thermally stable up to 500°C in the Composite-P4-SDS**,** so there is a temperature gain of 200°C for microcrystalline cellulose in the composite structure. The result is consistent with that of the XRD analysis (Figure 1b and Figure 1f). Consequently, the Composite-P4-SDS nanocomposite exhibits the best thermal stability since its degradation temperature increases by 100°C, compared to composite-P1, composite-P2, and composite-P3.

3.3. Thermal analysis DTA.

The DTA curves of the MgAl–LDH, CL, composite-P1, composite-P2, composite-P3, and composite-P4 samples are provided in Figure 3. The thermogram of MgAl–LDH (Figure 3a) shows that the decomposition of the solid took place in three distinct endothermic stages, corresponding to three mass losses. The first stage corresponds to the desorption of weakly bound or adsorbed water molecules from the outer faces of the crystals (a low-intensity peak at around 113°C, Δm = 10%) [29]. The second stage (peak around 228°C) was attributed to removing water molecules in the interfoliar domain (Δm = 7%). In the third step, carbonates are removed by decarboxylation of the right anions, and water molecules are removed by dehydroxylation of the sheets (Δm = 24%). It gives rise to an endothermic peak around 390°C [30].

The thermogram of the CL used (Figure 3b) shows an endothermic peak located at 75.8°C (Δm = 6%), corresponding to the elimination of physisorbed water molecules, and two other exothermic crystallization peaks located at 375.4°C and 479.1°C with mass losses of 55.7% and 9.2%, respectively, attributed to cellulose degradation [31]. The thermogram of the CL-LDH nanomaterial (Figure 3c) prepared according to protocol 1 (composite-P1) shows CL decomposition peaks with lower temperatures than cellulose alone. However, the peaks are broad, showing that the decomposition is slower. The thermograms of biocomposites synthesized by processes 2 and 3 (Figure 3d and Figure 3e) exhibit two exothermic peaks at 384°C and 476.7 °C, and at 312.43 °C and 455.45 °C, respectively. These peaks correspond to cellulose degradation. The biocomposite produced by process I (composite-P1), which has weakly polymerized microcrystalline cellulose (low PD), degrades at lower temperatures than observed in the other two processes. It indicates that it is less thermally stable. The elimination of water molecules in the interfollicular space of MgAl-LDH (peak around 228°C) occurs at a higher temperature for composite-P2, showing that these species become more stable when the MgAl–LDH is in a partially exfoliated structure. The endothermic peaks at 59°C and 203°C, caused by interlayer water and carbonate species between the MgAl-LDH layers, are very weak and cannot be seen compared to those of CL. It confirms the exfoliated structure found by the XRD analyses (CL is the main component).

The thermogram of the CL-MgAl–LDH nanomaterial produced using the ultrasound-assisted method (protocol 3) reveals exothermic CL decomposition peaks at 312°C and 455°C. The low-intensity endothermic peaks at 73 °C and 161 °C are caused by removing physi-sorbed water molecules and interfollicular space water molecules, respectively. A new exothermic peak was observed at 427 °C, which can be attributed to the additional phase (Figure 3e) observed on the diffractogram (Figure 1e) at 2θ = 37°. For all the developed nanomaterials, the disappearance of the endothermic peak at 389.68 °C corresponding to the release of water molecules by dehydroxylation and carbonates from MgAl–LDH indicates that these species are more strongly bound within the biocomposites and decompose at higher temperatures (typically above 500°C). The two exothermic peaks obtained on the thermograms of composite-P1 and composite-P3 (Figure 3c and Figure 3e) correspond to the decomposition of cellulose in the composite, for the carbonated cellulose/ Mg–Al biocomposite [31]. This degradation takes place at lower temperatures than those obtained for cellulose alone. The cellulose structure changed when clay particles were added, consistent with the XRD results (the amorphous phase disappeared in composite-P1, and another phase appeared in composite-P3).

Table 1. Thermal degradation parameters from DTA analyses of the synthesized biocomposites.

Composite	T onset (°C)	T max (°C)	T phase transition (°C)
MgAl–LDH	113	390	390
CL (cellulose)	76	479	479
P1	59	322	230
P2	67	384	477
P3	73	427	456
P4-SDS	68	468	467

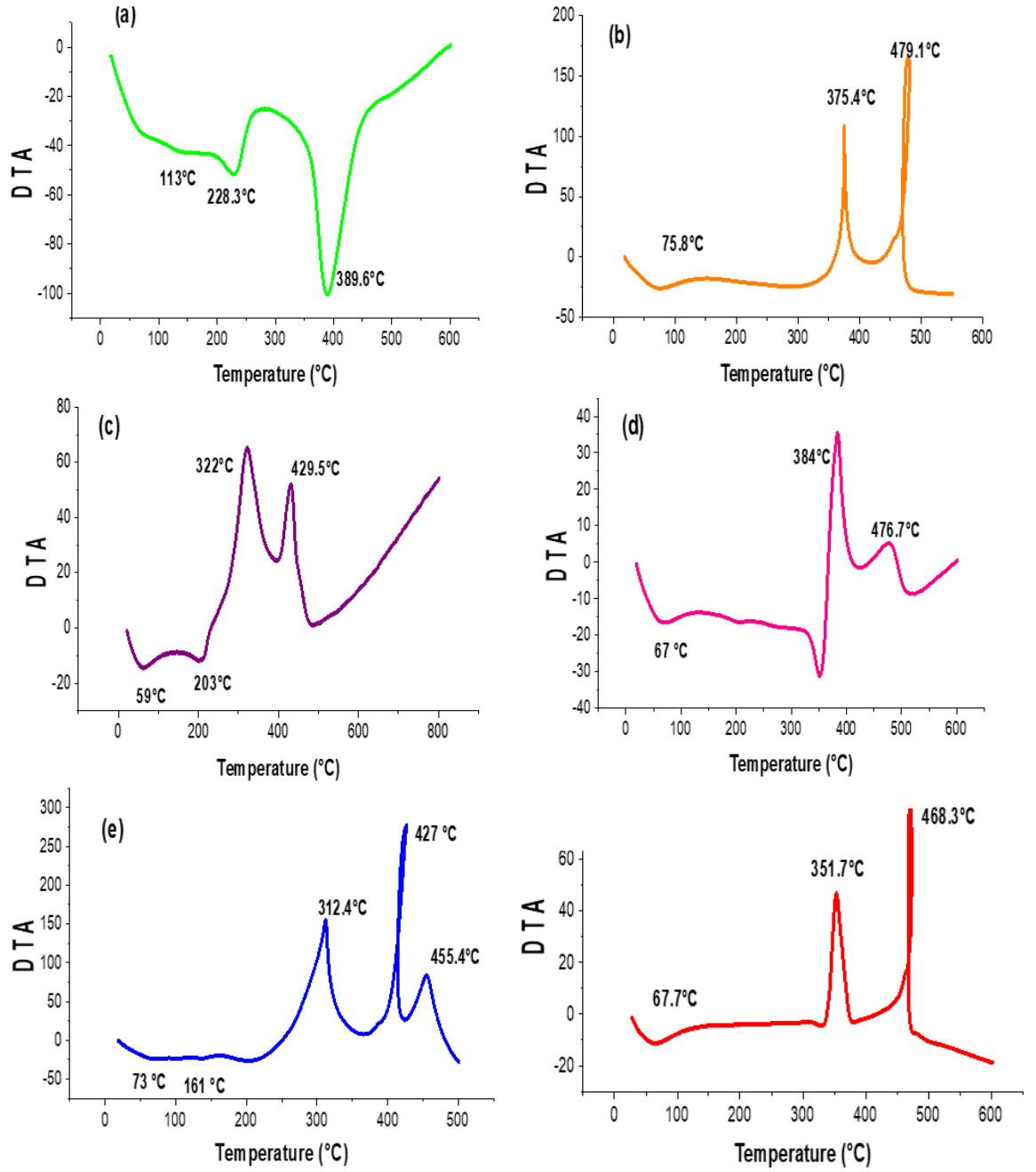

Figure 3. DTA curves for samples: **(a)** MgAl–LDH; **(b)** CL; **(c)** composite-P1; **(d)** composite-P2; **(e)** composite-P3; **(f)** composite-P4-SDS.

The DTA results, summarized in Table 1, show the thermal degradation parameters, such as Tonset, Tmax, and phase transition temperatures (°C), for MgAl–LDH, CL, and each biocomposite.

As a result, the observed variations in degradation temperatures may be attributed to structural modifications in the cellulose matrix and the dispersion state of MgAl–LDH particles within the composites. In composite-P1, the change in thermal behavior likely stems from the dispersion of MgAl–LDH within the polymer matrix, whereas in composite-P3, it may be related to the distribution of cellulose within the MgAl–LDH phase. For composite-P2, the initial degradation temperature of cellulose increased by about 10°C compared to pure cellulose, while the second degradation stage occurred at nearly the same temperature. This shift suggests a partially exfoliated structure, as evidenced by XRD analysis. In the case of composite-P4-SDS, which exhibited a fully exfoliated structure, no

endothermic peak corresponding to MgAl–LDH degradation was detected. This indicates enhanced thermal stability of MgAl-LDH in the nanocomposite, corroborated by the XRD results (Figure 1f). Moreover, the first exothermic peak associated with cellulose decomposition (Figure 3f) appeared broader, likely due to the overlapping degradation of sodium dodecyl sulfate (SDS).

4. Conclusion

Different procedures have been developed to create the biocomposites of microcrystalline cellulose/layered double hydroxide (CL/LDH) by dispersing MgAl–LDH clay nanofillers in microcrystalline cellulose solutions. X-ray diffraction (XRD), infrared spectroscopy, and DTA analyses confirmed the nanoscale dispersion of MgAl-LDH layers within the CL polymer matrix using various methods. The biocomposites P1 and P3 were characterized by peaks from both phases, MgAl–LDH and CL, whereas biocomposites P2 and P4-SDS exhibited partial and exfoliated structures, respectively, as evidenced by the decrease or disappearance of characteristic MgAl–LDH peaks. The thermal degradation behavior of the prepared composites was evaluated by calcining them at different temperatures and analyzing the resulting products by XRD, infrared spectroscopy, and DTA. Results revealed that the preparation method significantly influences the structural and thermal properties of the resulting nanomaterials. Among the tested materials, composite-P4-SDS exhibited the highest thermal resistance, showing an increase of 100 °C in degradation temperature compared to composites P1, P2, and P3, attributed to its exfoliated structure facilitated by SDS intercalation. For future work, mechanical performance evaluations and long-term thermal cycling studies are suggested further to assess the applicability and durability of these bioocomposites.

Author Contributions

Conceptualization, S.M. and H.Z.; methodology, S.M.; software, J.H.; validation, H.Z. and M.N.B.; formal analysis, J.H.; investigation, M.N.B.; resources, M.N.B.; data curation, S.M. and J.H.; writing original draft preparation, S.M. and H.Z.; writing review and editing, J.H. and M.N.B.; visualization, M.A.; supervision, M.N.B. All authors have read and agreed to the published version of the manuscript.

Institutional Review Board Statement

Not applicable.

Informed Consent Statement

Not applicable.

Data Availability Statement

Data supporting the findings of this study are available upon reasonable request from the corresponding author.

Funding

This research received no external funding.

Acknowledgments

The authors sincerely thank the Laboratory of Chemistry–Biology Applied to the Environment and the National Center for Scientific and Technical Research for their collaboration in this work.

Conflicts of Interest

The authors declare no conflict of interest.

Abbreviations

The following abbreviations are used in this manuscript:

Abbreviation	Definition
CL	Microcrystalline Cellulose
LDH	Layered Double Hydroxide
SDS	Sodium Dodecyl Sulfate
XRD	X-ray Diffraction
FTIR	Fourier-Transform Infrared Spectroscopy
DTA	Differential Thermal Analysis
MgAl-LDH	Magnesium-Aluminum Layered Double Hydroxide
P	Protocol
NFC	Nano-fibrillated Cellulose
CMC	Carboxymethylcellulose
PP	Polypropylene
PMMA	Poly(methyl methacrylate)
PLA	Poly(lactic acid)

References

1. Houssaini, J.; Naciri Bennani, M.; Arhzaf, S.; Mounir, C.; Alaqarbeh, M.; Ahlafi, H.; Amhoud, A. Solvent-Free Synthesis of Jasminaldehyde over Chitosan–layered Double Hydroxide Catalyst Assisted by Microwave Irradiation. *Arab. J. Chem.* **2023**, *16*, 105326, https://doi.org/10.1016/j.arabjc.2023.105326.
2. Hassan, T.; Salam, A.; Khan, A.; Khan, S.U.; Khanzada, H.; Wasim, M.; Khan, M.Q.; Kim, I.S. Functional Nanocomposites and Their Potential Applications: A Review. *J. Polym. Res.* **2021**, *28*, 36, https://doi.org/10.1007/s10965-021-02408-1.
3. Ates, B.; Koytepe, S.; Ulu, A.; Gurses, C.; Thakur, V.K. Chemistry, Structures, and Advanced Applications of Nanocomposites from Biorenewable Resources. *Chem. Rev.* **2020**, *120*, 9304–9362, https://doi.org/10.1021/acs.chemrev.9b00553.
4. Darwish, M.S.A.; Mostafa, M.H.; Al-Harbi, L.M. Polymeric Nanocomposites for Environmental and Industrial Applications. *Int. J. Mol. Sci.* **2022**, *23*, 1023, https://doi.org/10.3390/ijms23031023.
5. Chen, Z.; Aziz, T.; Sun, H.; Ullah, A.; Ali, A.; Cheng, L.; Ullah, R.; Khan, F.U. Advances and applications of cellulose bio-composites in biodegradable materials. *J. Polym. Environ.* **2023**, *31*, 2273-2284, https://doi.org/10.1007/s10924-022-02561-8.
6. Samir, A.; Ashour, F.H.; Hakim, A.A.A.; Bassyouni, M. Recent Advances in Biodegradable Polymers for Sustainable Applications. *npj Mater. Degrad.* **2022**, *6*, https://doi.org/10.1038/s41529-022-00277-7.
7. Yang, Q.; Wu, C.N.; Saito, T.; Isogai, A. Cellulose-Clay Layered Nanocomposite Films Fabricated from Aqueous cellulose/LiOH/urea Solution. *Carbohydr. Polym.* **2014**, *100*, 179–184, https://doi.org/10.1016/j.carbpol.2012.10.044.
8. Khan, S.B.; Alamry, K.A.; Bifari, E.N.; Asiri, A.M.; Yasir, M.; Gzara, L.; Ahmad, R.Z. Assessment of Antibacterial Cellulose Nanocomposites for Water Permeability and Salt Rejection. *J. Ind. Eng. Chem.* **2015**, *24*, 266–275, https://doi.org/10.1016/j.jiec.2014.09.040.
9. Delhom, C.D.; White-Ghoorahoo, L.A.; Pang, S.S. Development and Characterization of

Cellulose/clay Nanocomposites. *Compos. Part B Eng.* **2010**, *41*, 475–481, https://doi.org/10.1016/j.compositesb.2009.10.007.

10. Liu, A.; Berglund, L.A. Fire-Retardant and Ductile Clay Nanopaper Biocomposites Based on Montmorrilonite in Matrix of Cellulose Nanofibers and Carboxymethyl Cellulose. *Eur. Polym. J.* **2013**, *49*, 940–949, https://doi.org/10.1016/j.eurpolymj.2012.12.017.
11. Mekdad, S.; Mohamed Naciri Bennani Comparative Study of Different Protocols for the Preparation of Anionic Clay-Polymer Nanocomposite (Hydrotalcite-Cellulose) and Their Structural Properties. *Int. J. Innov. Res. Sci. Eng. Technol.* **2016**, *5*, 9861–9869, https://doi.org/10.15680/ijirset.2015.0506047.
12. Houssaini, J.; Naciri Bennani, M.; Ziyat, H.; Arhzaf, S.; Qabaqous, O.; Amhoud, A. Study of the Catalytic Activity of the Compounds Hydrotalcite Type Treated by Microwave in the Self-Condensation of Acetone. *Int. J. Anal. Chem.* **2021**, *2021*, 1551586, https://doi.org/10.1155/2021/1551586.
13. Jia, N.; Li, S-M.; Ma, M.-G.; Sun, R.-C.; Zhu, J.-F. Hydrothermal Synthesis and Characterization of Cellulose-Carbonated Hydroxyapatite Nanocomposites in NaOH–Urea Aqueous Solution. *Sci. Adv. Mater.* **2010**, *2*, 210–214, https://doi.org/10.1166/sam.2010.1086.
14. Mekdad, S.; Naciri Bennani, M.; Ahlafi, H. Elaboration d'un nanomatériau à partir d'une cellulose microcristalline et d'une Hydrotalcite Mg_2AlCO_3 [Elaboration of a nanomaterial from microcrystalline cellulose and a Hydrotalcite Mg_2AlCO_3]. *Mater. Environ. Sci.* **2014**, *5*, 2236–2243.
15. Mekdad, S.; Bennani, M.N.; Diouri, M. Effect of the Mg/Al Ratio and of the Rate of Reinforcement on the Synthesis of a Nanocomposite Cellulose/Hydrotalcite. *J. Adv. Chem.* **2014**, *5*, 2236–2243.
16. Ziyat, H.; Bennani, M.N.; Hajjaj, H.; Mekdad, S.; Qabaqous, O. Synthesis and Characterization of Crude Hydrotalcite Mg–Al–CO_3: Study of Thymol Adsorption. *Res. Chem. Intermed.* **2018**, *44*, 4163–4177, https://doi.org/10.1007/s11164-018-3361-9.
17. Houssaini, J.; Bennani, M.N.; Ziyat, H.; Arhzaf, S.; Zerhouni, J.; Alaqarbeh, M. Effect of Divalent Cations on the Basicity and Catalytic Performance of Layered Double Hydroxide Heterogeneous Catalyst in Microwave-Assisted Aldol-Condensation of Benzaldehyde with 1–heptanal. *Chem. Phys. Impact* **2024**, *8*, 100569, https://doi.org/10.1016/j.chphi.2024.100569.
18. Warmuz, K.; Madej, D. Synthesis and Evaluation of Mg-Al Hydrotalcite Formation and Its Influence on the Microstructural Evolution of Spinel-Forming Refractory Castables under Intermediate Temperatures. *J. Eur. Ceram. Soc.* **2022**, *42*, 2545–2555, https://doi.org/10.1016/j.jeurceramsoc.2022.01.009.
19. Vanitjinda, G.; Nimchua, T.; Sukyai, P. Effect of Xylanase-Assisted Pretreatment on the Properties of Cellulose and Regenerated Cellulose Films from Sugarcane Bagasse. *Int. J. Biol. Macromol.* **2019**, *122*, 503–516, https://doi.org/10.1016/j.ijbiomac.2018.10.191.
20. Jaffar, S.S.; Saallah, S.; Misson, M.; Siddique, S.; Roslan, J.; Lenggoro, W. Isolation and Characterization of Cellulose Nanocrystals from Solid Seaweed Wastes. *J. Adv. Res. Micro Nano Eng.* **2025**, *28*, 47–59, https://doi.org/10.37934/armne.28.1.4759.
21. Zhao, H.; Holladay, J.E.; Kwak, J.H.; Zhang, Z.C. Inverse Temperature-Dependent Pathway of Cellulose Decrystallization in Trifluoroacetic Acid. *J. Phys. Chem. B* **2007**, *111*, 5295–5300, https://doi.org/10.1021/jp070253f.
22. Valente, J.S.; Rodriguez-Gattorno, G.; Valle-Orta, M.; Torres-Garcia, E. Thermal Decomposition Kinetics of MgAl Layered Double Hydroxides. *Mater. Chem. Phys.* **2012**, *133*, 621–629, https://doi.org/10.1016/j.matchemphys.2012.01.026.
23. Ziyat, H.; Naciri Bennani, M.; Dehmani, Y.; Houssaini, J.; Allaoui, S.; Kacimi, R.; Hajjaj, H. Adsorptive Performance of a Synthesized Mg-Al Hydrotalcite Compound for Removal of Malachite Green: Kinetic, Isotherm, Thermodynamic, and Mechanism Study. *Int. J. Environ. Anal. Chem.* **2022**, *104*, 1072–1091, https://doi.org/10.1080/03067319.2022.2032006.
24. Ziyat, H.; Elmzioui, S.; Naciri Bennani, M.; Houssaini, J.; Allaoui, S.; Arhzaf, S. Kinetic, Isotherm, and Mechanism Investigations of the Removal of Nitrate and Nitrite from Water by the Synthesized Hydrotalcite Mg–Al. *Res. Chem. Intermed.* **2021**, *47*, 2605–2627, https://doi.org/10.1007/s11164-021-04414-w.
25. Houssaini, J.; Naciri Bennani, M.; Arhzaf, S.; Ziyat, H.; Alaqarbeh, M. Effect of Microwave Method on Jasminaldehyde Synthesis Using Solvent-Free over Mg–Al–NO_3 Hydrotalcite Catalyst. *Arab. J. Chem.* **2023**, *16*, 105316, https://doi.org/10.1016/j.arabjc.2023.105316.
26. Sain, M.; Panthapulakkal, S. Bioprocess Preparation of Wheat Straw Fibers and Their

Characterization. *Ind. Crops Prod.* **2006**, *23*, 1–8, https://doi.org/10.1016/j.indcrop.2005.01.006.
27. Alemdar, A.; Sain, M. Isolation and Characterization of Nanofibers from Agricultural Residues - Wheat Straw and Soy Hulls. *Bioresour. Technol.* **2008**, *99*, 1664–1671, https://doi.org/10.1016/j.biortech.2007.04.029.
28. Ul-Islam, M.; Khan, T.; Park, J.K. Nanoreinforced Bacterial Cellulose-Montmorillonite Composites for Biomedical Applications. *Carbohydr. Polym.* **2012**, *89*, 1189–1197, https://doi.org/10.1016/j.carbpol.2012.03.093.
29. Arhzaf, S.; Houssaini, J.; Naciri Bennani, M.; Alaqarbeh, M.; Bouachrine, M. Effect of Interlayer Anions on the Catalytic Activity of Mg-Al Layered Double Hydroxides for Furfural and Acetone Aldol Condensation Reaction. *Arab. J. Chem.* **2024**, *17*, 105412, https://doi.org/10.1016/j.arabjc.2023.105412.
30. Extremera, R.; Pavlovic, I.; Pérez, M.R.; Barriga, C. Removal of Acid Orange 10 by Calcined Mg/Al Layered Double Hydroxides from Water and Recovery of the Adsorbed Dye. *Chem. Eng. J.* **2012**, *213*, 392–400, https://doi.org/10.1016/j.cej.2012.10.042.
31. Islam, M.; Mishra, P.C.; Patel, R. Arsenate Removal from Aqueous Solution by Cellulose-Carbonated Hydroxyapatite Nanocomposites. *J. Hazard. Mater.* **2011**, *189*, 755–763, https://doi.org/10.1016/j.jhazmat.2011.03.051.

Publisher's Note & Disclaimer